## Deterministic control of magnetotactic bacteria via an analysis of their nanomagnetic structure

Noah Kent , 1,2,3,\* Colin Gates , 2,4 Bohdan Senyuk , 1,5 Jan Bart ten Hove , 2

Jeffrey Cameron, 6,2,7 and Ivan I. Smalyukh , 1,8,2,5

¹Department of Physics, University of Colorado, Boulder, Colorado 80309, USA
²Renewable and Sustainable Energy Institute, National Renewable Energy Laboratory

and University of Colorado, Boulder, Colorado 80309, USA
³Research Laboratory of Electronics, Massachusetts Institute of Technology, Cambridge, Massachusetts 02139, USA
¹Department of Chemistry and Biochemistry, Loyola University Chicago, Flanner Hall, Chicago, Illinois 60660, USA
¹International Institute for Sustainability with Knotted Chiral Meta Matter, Hiroshima University, Higashihiroshima, Japan
¹Department of Biochemistry, University of Colorado, Boulder, Colorado 80309, USA
¬National Renewable Energy Laboratory, Golden, Colorado 80401, USA
¹Department of Electrical, Computer and Energy Engineering, Materials Science Engineering program and Soft Materials Research Center, University of Colorado, Boulder, Colorado 80309, USA

(Received 11 March 2025; accepted 1 August 2025; published 17 October 2025)

Magnetotactic bacteria are microorganisms with magnetite organelles that have been shown to be responsive to external magnetic fields. Despite their study for several decades, a complete theoretical understanding that connects the magnetic structure of these bacteria to their external magnetic field response has not been conclusively resolved. Combining nanomagnetic simulations with optical and transmission electron microscopy, it is shown that the response of magnetotactic bacteria to a strong external magnetic field is dependent on the internal arrangement of the magnetite organelles and can be understood at a fundamental level. With this information, nonpolar and polar velocity vector fields can be observed and defined in the bacteria's movement. By directly manipulating the bacteria with external magnetic fields, we are able to control large in-phase groups of bacteria, have precise control of individual bacterium trajectories, and generate structures with a topological charge in both their polar and nonpolar velocity vector fields. Being able to directly control these bacteria with external magnetic fields opens up the possibility of using them as self-propelled microrobots with biomedical applications, such as targeted magnetic hyperthermia and drug delivery.

## DOI: 10.1103/ggl8-44wg

I. INTRODUCTION

Magnetosomes are magnetite or greigite magnetic nanoparticle (MNP) containing bacterial organelles, which are synthesized by diverse magnetotactic bacteria, such as Magnetospirillum magneticum (hereafter M. magneticum) under study here, via biomineralization of magnetic elements [1-3]. It is thought that magnetotactic bacteria produce magnetosomes in order to facilitate navigation to an environment with appropriate oxygen levels [1-4]. Much work has been done to understand and control the behavior of magnetotactic bacteria in microfluidic controllers, under sheer force of obstacles, collective bacteria swarming behavior, and chemotaxis [5,6]. Previous work on the behavior of magnetotactic bacteria in magnetic fields has assumed that the magnetic structure is a rigid dipole fixed along the bacterium's long axis; this axis is also the direction in which the bacterium propels itself [1-3,6-10]. Such models have successfully elucidated the behavior of these bacteria in rotating external fields and magnetic field gradients. Some models allow for flexibility of the magnetic moment relative to the forward direction [10]. However, all existent models do not successfully explain the behavior of an individual

bacterium in the presence of a uniform magnetic field, do not allow for direct directional control over a set of bacteria, and do not address the inherent energetic degeneracy present in uniaxial magnetic systems [6–10].

Additionally, in recent years, there has been significant research on topological structures, such as skyrmions and hopfions, in both magnetic [11,12] and soft matter liquid crystal systems [13,14] due to their stability and technological potential. Magnetic systems and soft matter systems typically differ in the nature of their order parameter: Magnetic systems usually have a polar order parameter and soft matter systems usually have a nonpolar (axial) order parameter [11–13]. No topological structures have been observed in magnetotactic bacteria despite them exhibiting both magnetic and soft matter properties.

Magnetotactic bacteria have had some of their magnetic properties elucidated. In magnetite, the individual magnetic nanoparticles have a complex ferrimagnetic magnetic coupling between two sublattices A and B, where A-A coupling is ferromagnetic, B-B coupling is antiferromagnetic, and A-B coupling is antiferromagnetic [15]; see Fig. S5 in the Supplemental Material [16] for further clarification. At these size scales, the individual MNPs are effectively approximated as superparamagnetic or single-domain ferromagnetic and have cubic anisotropy due to a combination of the MNP's

<sup>\*</sup>Contact author: nkent@mit.edu

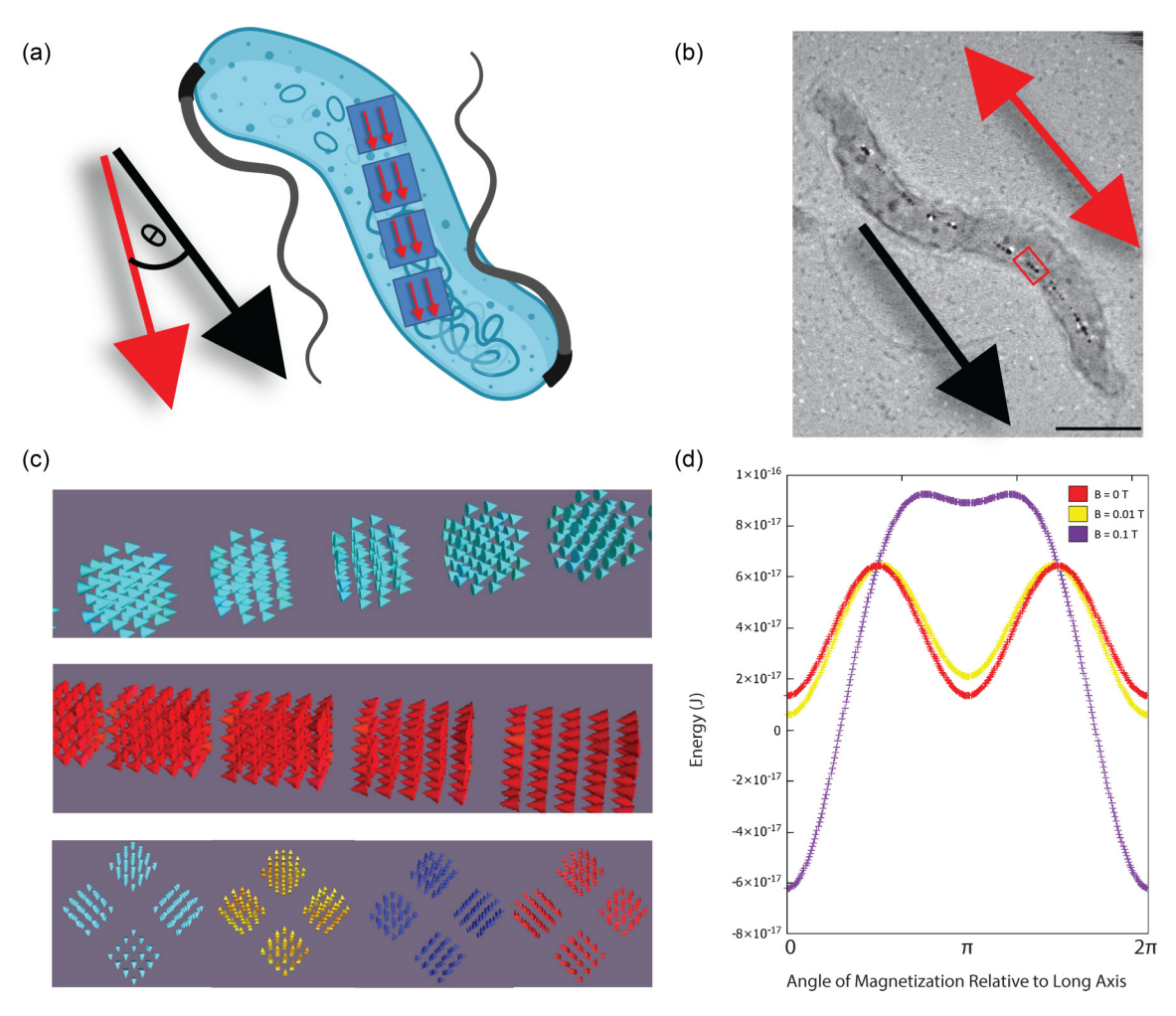


FIG. 1. Magneto-structural properties of *M. magneticum*. (a) Schematic of a magnetotactic bacterium showing its flagella, which push the bacterium forward in the direction of the black arrow, the internal magnetization of the MNPs (red arrow), and the angle  $\theta$  between the forward direction of the bacterium and the magnetization of the MNPs. (b) TEM image of a bacterium with magnetosomes (several are highlighted in a red box) arrayed in a straight line. The red arrows represent possible magnetization directions of the MNP chain. The black arrow represents a possible forward direction of the bacterium. (c) Lowest-energy configurations for arrangements of spherical (top) and square (middle) MNPs arranged in a line and showing behavior similar to that of a uniaxial ferromagnet. The bottom shows four degenerate configurations for particles arranged with square symmetry, having square anisotropy. (d) Magnetization as a function of angle relative to the long axis of a bacterium for a chain of 18 MNPs in a uniaxially aligned bacterium where the magnetization is allowed to rotate freely relative to the structure of the bacterium and the magnetic field is aligned with the forward direction of the bacterium ( $\theta = 0$ ). Magnetic field is applied along  $\theta = 0$ .

cubic shape and inherent crystalline cubic anisotropy [17–19]. Large swarms of the bacteria have experimentally been found to have uniaxial anisotropy [17,18,20]. Most of the time in *M. magneticum*, the magnetosomes are arrayed in approximately a straight line along the major axis of the bacterium, as in Figs. 1(a) and 1(b), but it is important to note that there is a wide variety of magnetotactic bacteria which produce magnetosomes of different shapes, sizes, and arrangements [1,2,21,22]. There is also some variation of magnetosomes within a single strain of bacteria (i.e., number, size of magnetosomes, how they are arranged) [17]; see Fig. S1 in the Supplemental Material [16].

From a fundamental physics perspective, arrangements of nanomagnets interacting with each other are very well understood both experimentally and theoretically. The magnetic properties of the individual nanomagnets are determined by their shape, size, and elemental composition. The collective magnetic structure of the system is determined by the properties of the individual nanomagnets combined with how they are arrayed with each other [23–25] and are determined by the fundamental nanomagnetic energies involved: direct exchange (ferromagnetic, antiferromagnetic), shape anisotropy, and dipole-dipole interaction between adjacent nanomagnets [23–25].

Here, state-of-the-art simulations of magnetosomes, based on the real distributions of the magnetite nanoparticles observed in transmission electron microscopy (TEM), and dark-field optical microscopy with *in situ* magnetic fields allow us to explain previously anomalous behavior in the bacteria [7,8], control large in-phase groups of bacteria directly with an external uniform magnetic field, selectively change the topological parameter space from polar to nonpolar, and generate topological structures in both the polar and the nonpolar velocity vector fields of the bacteria.

### II. MATERIALS AND METHODS

### A. Bacteria growth and storage

Magnetospirillum magneticum ATCC 700264 was purchased from the American Type Culture Collection (Virginia, USA) as frozen stock. M. magneticum was revived by unfreezing and cultured at 30 °C in crimp-sealed airtight vials wrapped in aluminum foil to prevent light exposure. Cultures were grown in ATCC Revised Magnetic Spirillum growth medium (ATCC Medium 1653) without headspace gas to maintain microaerobic conditions. All bacteria were derived from the same lineage.

#### B. MuMax3 simulations

MuMax3 [26] was used for all simulations of the magnetosome chains. Realistic parameters for the magnetite were used: saturation magnetization  $M_s = 300 \text{ kA/m}$ , exchange stiffness  $A = 13 \times 10^{-12}$  J/m, and Landau-Lifshitz damping constant  $\alpha = 0.2$  [27,28]. Mesh sizes were cubes with edge lengths of either 2 or 3 nm. Three different types of simulations were performed. In the different types of simulations, particle size, spacing, and shape were varied and are as follows: (1) simulations where the MNP chains were allowed to relax under the Landau-Lifshitz micromagnetic formalism, at 0 and 300 K, without an external field [Fig. 1(c)]. This establishes the naturally occurring state of the magnetization present in the bacteria; for chains of particles aligned in a straight line, the magnetization is uniaxially ferromagnetic and will point up or down the chain. (2) Simulations where the magnetization is rotated relative to the length of the uniaxially ferromagnetic MNP chain (Fig. 1(d) and Figs. S2 and S3 in the Supplemental Material [16]). The external magnetic field is also varied in these simulations. These simulations show that even in an external magnetic field, it is unlikely that thermal fluctuations at room temperature will flip the internal magnetization, and further confirm that these chains are uniaxial ferromagnetic. (3) Simulations where the entire chain of MNPs rotates relative to the external magnetic field (Fig. 2(a), and Fig. S4 in the Supplemental Material [16]). These simulations show that in external fields greater than 0.001 T, the internal dipole moment of the bacteria will always align with the external field, and for fields over 0.001T, uniaxially aligned bacteria will move (anti)parallel to the applied field, ignoring fluid resistance and thermal effects. The statements about deterministic behavior of the bacteria at room temperature are for chains of six or more magnetosomes.

## C. Microscopy and magnetic field setup

TEM samples were prepared by drop-casting  $10~\mu L$  of bacteria in solution on 300 mesh carbon-coated copper grids (EMS, Hatfield, PA, USA). After 30 seconds, excess liquid was removed and the grids were dried by exposure to air for at least another 30 seconds. The samples were imaged in a Tecnai ST20 200 kV electron microscope for TEM.

Olympus IX-81 and IX-83 microscopes were used in both bright-field and dark-field mode. Custom three-dimensional (3D) printed holders for cylindrical and doughnut-shaped magnets were designed to generate magnetic fields that were either uniform over the region viewed in the microscope or

a magnetic field which should produce topological structures in the bacterial velocity fields. Magnetic field shapes were analytically calculated and magnetic field strength was experimentally measured with a FW Bell 9900 Multi-Channel Gaussmeter with an accuracy of  $\pm 1\%$ . Field strength measurements were done over the central  $2 \times 2$  cm region, checking for field strength and uniformity. For a uniform in-plane magnetic field, two cylindrical magnets (magnetized along the length of the cylinder) were aligned such that their magnetizations were pointing in the same direction and produced a uniform field of 0.01 T. For a uniform out-of-plane magnetic field, the 3D printed holder aligned two doughnut magnets with the microfluidic slide placed exactly equidistant between them. This produces a uniform out-of-plane magnetic field of 0.049 T. All magnets were NdFeB magnets purchased from K+J Magnetics (PA, USA).

Ibidi  $\mu$ -Slide I Luer slides with a channel thickness of 200  $\mu$ m were used for all microscopy experiments, except for the experiment with the current-carrying wire. An Ibidi  $\mu$ -Slide 2 Well was used for the experiment with the current-carrying wire.

In order to generate a relatively uniform in-plane magnetic field that could be varied in any in-plane direction, two wirewrapped soft iron core electromagnets were arranged at a 90-degree angle relative to each other in the imaging plane of the Olympus IX-81 microscope. This setup produced a magnetic field which, while not perfectly uniform, had minimal variation near the imaging region. The magnetic field was measured in a  $2\times 2$  cm square centered on the imaging region and was found to be 0.006–0.0057 T. The magnetic field was measured over the actual imaging region by holding the Gaussmeter in the microscope gantry and measuring at the four corners of the central region (an approximately  $500\times500~\mu m$  square). No variation in the 0.0058 T field was found.

Magnetic field strength calculations, and the resultant graphs, were done in python using exact analytical solutions for fields generated from finite cylindrical solenoids [30]

#### D. Determining bacterial (non)polar velocity vectors

Bacterial motion was tracked with the FIJI plugin mosaic [42]. The direction of motion was extracted from tracked data; this directly gives polar velocity vectors. To construct nonpolar velocity vectors, the extracted directional angle is calculated mod $\pi$ , e.g.,  $\frac{3}{2}\pi$  goes to  $\frac{1}{2}\pi$ . To determine the average directional vectors, a circular mean is calculated for both polar and nonpolar velocity vectors:

$$\bar{\theta} = F\left[\frac{1}{n}\sum_{i=1}^{n} \operatorname{Sin}(\theta_i), \frac{1}{n}\sum_{i=1}^{n} \operatorname{Cos}(\theta_i)\right],\tag{1}$$

where

$$F[x, y] = \begin{cases} \arctan(\frac{x}{y}) & \text{if } y < 0\\ \arctan(\frac{x}{y}) + x & \text{if } y > 0 \end{cases}, \tag{2}$$

and  $\theta_i$  are the *n* measured directional velocity vectors. This average angle was then checked against the measured angular distribution of velocity vectors to confirm that there is a mode

in the angular velocity vector distribution and it approximately agrees with the calculated average angle.

#### E. Topological charge calculation

Most topological structures in liquid crystals and magnetic systems are defined as a mapping of a closed membrane from a three-dimensional parameter space to a two- or three-dimensional physical space. Since the magnetotactic bacteria in this study only move in-plane, a closed membrane is mapped from a two-dimensional parameter space to a two-dimensional real space [14,31]. Additionally, the bacterial velocity vector fields  $\mathbf{v}$  that we observed can be approximated as only a function of in-plane angle  $\tau$  in the form  $\mathbf{v}(\tau) = [\cos\theta(\tau), \sin\theta(\tau)]$ . As such, the topological charge, i.e., the winding number (W), calculation is greatly simplified to [31]

$$W = \frac{1}{2\pi} \int_{0}^{2\pi} d\tau \, \partial_{\tau} \theta. \tag{3}$$

The physical interpretation is that for every in-plane rotation made by  $\mathbf{v}$ ,  $\mathbf{W}$  increases by one.

This calculation is done specifically for a polar velocity vector; for nonpolar velocity vectors, the order parameter space only spans from 0 to  $\pi$ . However, convention in other nonpolar systems (e.g., liquid crystals [14]) dictates that we wrap the parameter space twice for a winding number of 1. Therefore, the topological charge calculation for polar systems holds for nonpolar systems.

### III. RESULTS

# A. TEM measurements of magnetosomes and magnetic simulations

In order to simulate and understand the magnetic properties of the magnetotactic bacteria, the physical arrangement of the magnetic elements within the bacteria must be determined. TEM measurements of M. magneticum show approximately cubic MNPs with a side length ranging from 20 to 60 nm, with an average of  $30 \pm 2$  nm, in agreement with previous observations of magnetosomes [1,2,7,8]. The individual nanoparticles have cubic anisotropy and are single-domain ferromagnetic or superparamagnetic at room temperature depending on the exact shape and size of the individual particle [17,32–35].

The MNPs are primarily arrayed in straight lines running along the long axis of the bacterium; see Fig. 1(b). However, there is variation in these arrangements: some bacteria have MNPs that are in straight lines but not parallel to their long axis, some have magnetosomes that are not arrayed in straight lines, and some do not have any MNPs; see Fig. S1 in the Supplemental Material [16]. In order to generate a quantitative and predictive framework that describes the behavior of magnetotactic bacteria in a magnetic field, a wide variety of simulations were performed using realistic parameters for magnetite nanoparticles (see Sec. II for parameters) [27,28].

Magnetic simulations of these arrangements of MNPs show that for an array of MNPs in a chain, it is always energetically favorable to have the magnetization aligned (anti)parallel to the length of the chain; see Fig. 1(d). There is an energetic degeneracy between both directions of magnetization along the length of the chain in no external magnetic

field; see Fig. 1(d), red line. In an external magnetic field, this degeneracy is broken and there is an energetic preference for the magnetization to align with the external field. Nonetheless, it is possible for the magnetization to get stuck in a metastable energy minimum and align antiparallel to the applied field; see Fig. 1(d). However, in a liquid medium, the bacteria are free to rotate so it is physically realistic to consider the energy of a bacterium with a fixed dipole moment (relative to the bacterium) as a function of angle with the external magnetic field; see Fig. 2(a) and Fig. S4 in the Supplemental Material [16]. In this case, the bacterium's magnetization will always rotate to align parallel to the applied field in a large magnetic field (B > 0.001 T). In a uniform magnetic field, the dipole moments of the magnetosome chains will experience a torque and, assuming the magnetosomes are fixed relative to their host bacterium, the bacterium itself will experience a torque aligning its dipole moment with the external field. This is ignoring restive effects of the medium the bacteria are in and any thermal fluctuations. We can quantify thermal fluctuations at room temperature  $[K_B T \ (T = 298 \ \text{K}) = 4.1 \times 10^{-21} \ \text{J}]$ , and approximate if a bacterium is subject to such fluctuations if the anisotropy energy barrier is smaller than the thermal energy at room temperature. For the Earth's magnetic field (0.00003 T), bacteria with six or fewer closely packed magnetosomes will be subject to thermal fluctuations, but for strong fields (>0.001 T), even two closely packed magnetosomes will be sufficient to ignore thermal fluctuations and have their collective dipole moment always align with the external magnetic field, along the length of the MNP chain. Additionally, in a strong field, the spacing between magnetosomes can be significantly varied (up to hundreds of nanometers) and uniaxial ferromagnetic behavior will still be observed, as long as the magnetosomes are in a straight line (a magnetosome chain); see Fig. 2(a) and Figs. S2 and S3 in the Supplemental Material [16].

Simulations show that while the magnetic properties of the individual MNPs can differ between particles, depending on their size and shape, the collective magnetic structure is more robust and is determined by how the particles are arrayed. For example, in a chain of 18 MNPs which are cubes, the individual MNPs have cubic anisotropy, but when arrayed together, the collective structure has uniaxial anisotropy. The same collective behavior is observed for a chain of 18 MNPs regardless of whether the individual MNPs are spheres (individual MNPs have no anisotropy) or rectangles (individual MNPs have uniaxial anisotropy); see Fig. 1(c), top and middle. This is in agreement with nanomagnetic experiments that show that collections of magnetic nanoparticles arrayed together can have robust static magnetic properties independent of whether individual MNPs have small deviations in anisotropy or even if they are superparamagnetic [23–25]. It is also possible for the magnetosomes to be arrayed such that the bacteria do not behave like a uniaxial ferromagnet, for example, if the magnetosomes are arrayed with square symmetry [Fig. 1(c), bottom] or triangular symmetries.

Given all this information and taking into account that the bacteria propel themselves in the direction of their long axis, the following statements can be made about magnetotactic bacteria in a strong, >0.001 T, uniform magnetic field: (1) For a bacterium with a chain of magnetosomes parallel to its

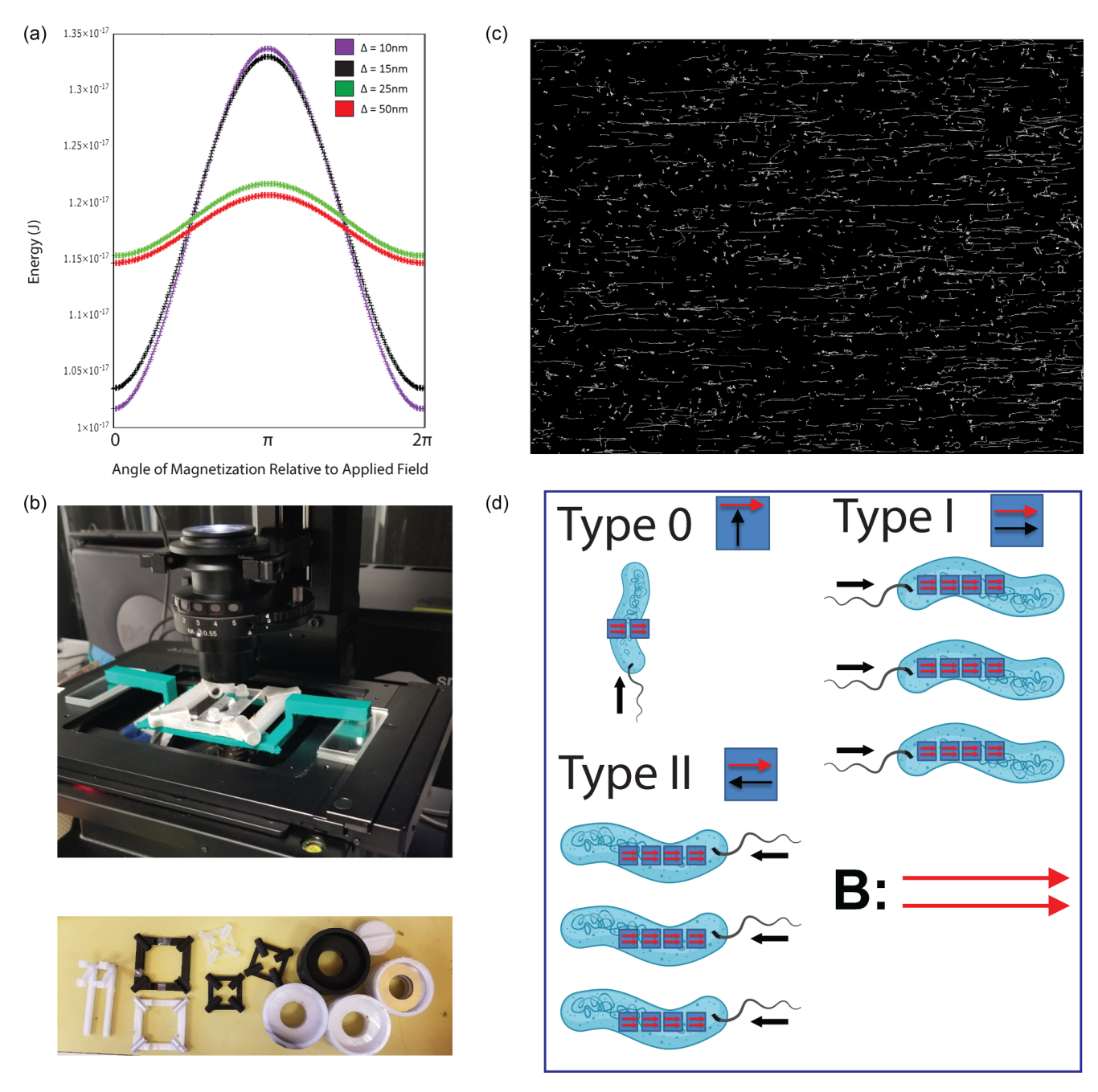


FIG. 2. Response to uniform magnetic fields. (a) Energy as a function of the relative angle between M and B (0.005 T applied along  $\theta=0$ ) where the chain of magnetosomes is allowed to rotate relative to the applied field, but its magnetization is fixed in the lowest-energy state.  $\Delta$  shows edge-to-edge spacing of magnetosomes. (b) Experimental setup for optical microscopy (top) using custom 3D printed holders for permanent magnets (bottom) in order to generate uniform or highly divergent fields. (c) Particle tracking of magnetotactic bacteria for 30 seconds in a uniform magnetic field applied along the x axis. (d) Schematic depiction of bacteria undergoing phase separation in a thin, narrow channel. Bacteria of type I (see the Supplemental Material, video SV3 [16]) will move in the direction of the applied field and build up on one side of the channel, and bacteria of type II (see the Supplemental Material, video SV4 [16]) will move antiparallel to the applied field and build up on the other side of the channel. Bacteria whose moment is not uniaxially aligned (type 0) will move up and down the length of the channel.

long axis, it will move (anti)parallel to the applied field. It is just as likely the bacterium will move parallel or antiparallel to the applied field as it is energetically equivalent for their internal dipole moment to be aligned with the forward or backwards direction of the bacterium. (2) For a bacterium where there is some angle  $\theta$  between its long axis and the chain of magnetosomes, it will move (anti)parallel to a line

that is at a  $\theta$  angle relative to the field. This explains the anomalous behavior previously seen where bacteria would move orthogonal or at a large angle to an applied magnetic field [7]. (3) For a bacterium where there is no energetic difference between multiple magnetization directions or for a bacterium which has no magnetosomes, they will move independently of an applied uniform field.

Since the magnetic properties of the bacterium are primarily dependent on the physical arrangement of collective groups of magnetosomes, we can predict the magnetic behavior of individual bacteria in a strong uniform magnetic field by observing the physical arrangement of the MNPs in the bacterium. Using TEM, bacteria can be placed into one of three categories, dependent on the observed physical arrangement of the magnetosomes in the bacteria: (1) likely uniaxial ferromagnetic parallel to the bacterial long axis [Fig. 1(a)], (2) not aligned uniaxially ferromagnetic, and (3) no magnetosomes (see Fig. S1 in the Supplemental Material [16]). We expect bacteria in category (1) to align (anti)parallel with the externally applied field; in category (2) to move at a high angle relative to the applied field or have multiple degenerate directions they can switch between; and in category (3) to not be affected by the externally applied field. As such, we can only deterministically predict the behavior of bacteria in category (1) and we expect them to align parallel and antiparallel, in equal amounts, to an external magnetic field. 84  $\pm$  4% (N = 100) of the bacteria were found to be in category (1) from TEM measurements. Bacteria that fit into categories (2) or (3) will be referred to as type 0 from this point on. Bacteria in category (1) will be referred to as type I if their forward direction and magnetic dipole moment are parallel with each other and type II if their forward direction and magnetic dipole moment are antiparallel to each other.

# B. Behavior of magnetotactic bacteria in a uniform magnetic field

The bacteria were confined to a 200-µm-thick microfluidic channel and a uniform in-plane magnetic field was applied by placing the bacteria in a 3D printed holder; see Fig. 2(b), bottom. Two cylindrical NdFeB magnets are aligned with this holder such that a uniform field of 0.01T is generated over the entire imaging region. This field is several orders of magnitude stronger than the Earth's magnetic field and sufficient to ignore thermal fluctuations for a MNP chain with six or more magnetosomes. When the field is applied to the sample, 87  $\pm$ 2% (N = 13548) of the bacteria align and move parallel or antiparallel to the externally applied field; see Fig. 2(c). This matches very well with our measurements from TEM that show 84% of the bacteria have aligned uniaxial anisotropy. There is an almost equal likelihood that bacteria move parallel,  $52 \pm 2\%$ , or antiparallel,  $48 \pm 2\%$ , to the applied field. This is expected since simulations and theory predict that there is an energy degeneracy between the magnetic moment of the magnetosomes aligning with or against the forward direction of the bacteria. Hence, when in a strong uniform magnetic field, the bacteria have a well-defined nonpolar velocity vector that is parallel to the applied field; see Fig. 2(c) and video SV1 in the Supplemental Material [16].

To test the effects of a uniform out-of-plane magnetic field on the bacteria, two doughnut-shaped magnets were aligned in a 3D printed holder [Fig. 2(b), bottom], such that the area observed in the microscope is a highly uniform out-of-plane magnetic field. In the thin slide sample, the out-of-plane magnetic field forces the bacteria into (anti)parallel alignment with the applied field. This arrests the motion of the bacteria since they are confined to a thin slide and cannot move up or down

(see video SV2 in the Supplemental Material [16]); this also acts as confirmation that the bacteria's velocity vector is confined to a two-dimensional plane when in the thin microfluidic slide. Further tests using thinner channels (100  $\mu$ m, ~20  $\mu$ m) prevent all bacterial motion, also confirming that the 200- $\mu$ m-thick channel approximately confines the bacteria velocity to two dimensions. Therefore, when considering topological structures in the bacteria, our order parameter space has a dimensionality of two and the real space is also two dimensional. See Sec. II for more details.

In a strong uniform magnetic field, we do not expect fluctuations of the magnetic dipole moment relative to the forward direction of the bacteria. Hence, in a confined channel, the bacteria can be physically separated depending on how their magnetic dipole moment is oriented relative to their forward direction by applying a uniform magnetic field and waiting; see Fig. 2(d). For aligned uniaxial bacteria, there should be a buildup on either side of our thin microfluidic slide; one side will have bacteria whose dipole moment is aligned parallel to their forward direction (type I) and the other side will have bacteria with their internal magnetic moment aligned antiparallel to their forward direction (type II); see Fig. 2(d). The other bacteria with magnetosomes which are not uniaxially aligned, i.e., type 0, will move up and down the length of the channel and will also be separated out; see Fig. 2(d). In Fig. 2(d), even though the bacteria have two flagella, only one flagella is shown in the figure to clearly indicate a forward

Phase separating the bacteria in an electromagnet allows for direct control over large groups of in-phase bacteria by changing the direction of the uniform magnetic field; see videos SV3 and SV4 in the Supplemental Material [16]. Both type I and type II bacteria can be fully controlled and behave as expected, with type I propelling themselves along the magnetic field direction and type II moving opposite to the applied field. Post-phase separation, all of the bacterial movement can be accounted for and falls into one of three categories: (1) immobile or dead bacteria, (2) bacteria without magnetosomes (unaffected by external field), or (3) uniaxial aligned ferromagnetic moving (anti)parallel to the externally applied field. Hence, post-phase separation, the bacteria have a well-defined polar velocity vector.

Post-phase separation, individual bacteria can also be guided with arbitrary control, e.g., to write "CU"; see Fig. 3(a). In Fig. 3(a), an individual bacterium, of type I, was used to write a "C" by manually varying the magnetic field direction. Another bacterium, of type II, was used to write a "U" by preprogramming the alignment of the external magnetic field to be at an angle of  $\frac{\pi}{2}$ , 0,  $-\frac{\pi}{2}$  relative to the horizontal direction. In Fig. 3(b), the magnetic field direction (red) is given at the different points in the bacterium's motion. The bacterium's polar velocity vector is shown in black. For clarity, in uniform magnetic fields, the magnetic field itself generates no net force on the bacteria (only a torque) and the bacteria are self-propelled.

# C. Behavior in nonuniform magnetic fields and topological structures in (non)polar velocity fields

Ferromagnets, ferrimagnets, and paramagnets experience a force in a nonuniform magnetic field such that  $\tilde{F} = \vec{\nabla}(\tilde{m} \cdot \tilde{B})$ ,

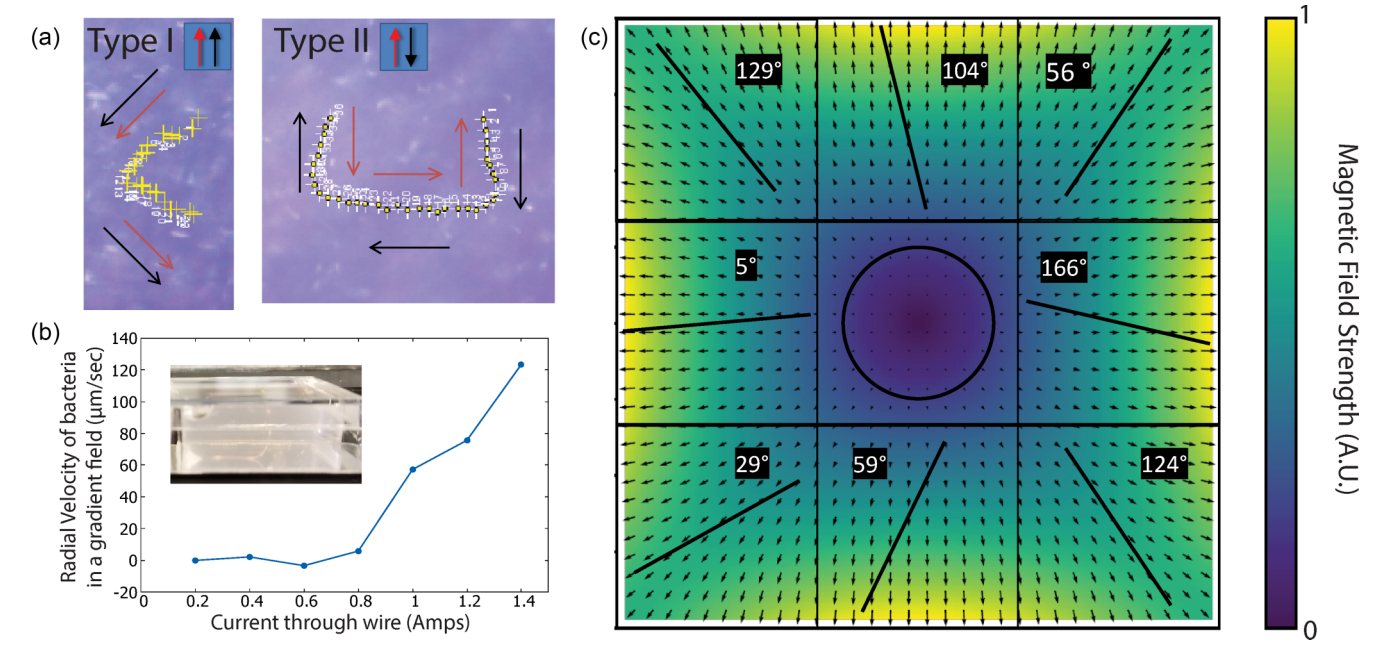


FIG. 3. Response to varying magnetic fields. (a) Left: bacterium of type I writing "C" via manual control of the magnetic field. Right: bacterium of type II used to write "U" with a preprogrammed magnetic field alignment of  $-\pi/2$ , 0,  $\pi/2$  relative to the horizontal direction. Red lines show the direction of the external magnetic field; black lines show the polar velocity vector of bacterium. (b) Velocity vs current for bacteria in a magnetic field gradient generated by a 63-µm-diameter wire threaded vertically through a box of bacteria (shown in inset). Bacteria are drawn radially inward due to the magnetic field gradient generated by the wire. (c) Formation of nonpolar topological structure with W=1 in the velocity vectors of magnetotactic bacteria with a length greater than 6 µm. An angular average was taken over  $400 \times 400$  µm areas, represented by the black squares. In the center, the bacteria were oriented randomly; therefore, the order parameter vanishes in the center. The underlay shows the analytically calculated magnetic field strength and direction.

where  $\tilde{F}$  is the force,  $\tilde{m}$  is the magnetic dipole moment of the material, and  $\tilde{B}$  is the magnetic field.

This means that in a magnetic field gradient, all bacteria with magnetosomes and magnetotactic bacteria (independent of type) will be drawn to the stronger magnetic field. Bringing a NdFeB magnet near an Eppendorf tube containing the magnetotactic bacteria shows that all bacteria with magnetosomes are attracted to the permanent magnet regardless of type; see video SV5 in the Supplemental Material [16]. The closer the permanent magnet is to the bacteria, the larger the attractive force since the field gradient is larger near the magnet's surface. Macroscopically, the behavior of the bacteria is indistinguishable from iron filings or any other ferromagnetic material suspended in liquid and subjected to a NdFeB magnet.

To further quantify the bacteria's behavior in magnetic field gradients, a thin (63-µm-diameter) insulated copper wire was threaded through a 9-mm-tall microfluidic well; see Fig. 3(b). The magnetic field generated by a current-carrying wire is  $\vec{B} = (\frac{\mu_0 I}{2\pi r})\hat{\varphi}$ , where I is the current in the wire, r is the radial distance from the wire, and  $\mu_0$  is the magnetic permeability of free space. Therefore, the magnetic field gradient and force scales linearly with the current.

A magnetic dipole would experience a force radially inward towards the wire. At low current values, there is no change in the behavior of the bacteria (the self-propelling nature of the bacteria dominates) until approximately 0.8 A, at which point the bacteria are drawn radially inward towards the wire; see Fig. 3(b). As the current through the wire in-

creases, the bacteria experience a larger force and are drawn radially inward with increasing speed; see video SV6 in the Supplemental Material [16] and Fig. 3(b).

Considering the bacteria are drawn radially inward towards the wire throughout the thickness of the cell, their polar velocity vector has a topological charge of 1. This is unsurprising as the wire acts as a "sink" for the bacteria. This is similar to how positively and negatively charged particles have topological charge  $\pm 1$  and are sources or sinks for electric field lines. There is a noticeable buildup of bacteria on the wire as time progresses.

In order to generate a nonpolar topological structure in the bacteria's velocity vector, another thin microfluidic slide was placed in an inverted quadrupole magnetic field generated by permanent magnets; see Fig. 2(b). This results in very weak magnetic field and magnetic field gradients near the center of the microfluidic slide, and a field magnitude of zero at the exact center. For small bacteria with a low number of magnetosomes, thermal effects dominate and they move randomly relative to the magnetic field. In order to observe the effects of the magnetic field on the nonpolar velocity vector of the bacteria, only bacteria over 6 µm in length with multiple visible magnetosomes are considered because simulations show that longer chains of magnetosomes are less affected by thermal fluctuations and are more responsive to an external magnetic field. In the central region of the slide a well-defined nonpolar velocity vector, parallel to the magnetic field lines, can be spatially mapped; see Fig. 3(c). However, near the exact center of the magnetic field setup, the long bacteria no longer have a well-defined nonpolar velocity vector and are seen to orient randomly to each other; see Fig. 3(c). Smoothly connecting the experimental nonpolar velocity vectors and calculating the topological charge in the nonpolar director field of the system results in a winding number of 1. The topological structure can be observed with large quantities of small bacteria by measuring 2–4 cm away from the 0-field point, where the magnetic field is stronger; see video SV7 in the Supplemental Material [16].

#### IV. DISCUSSION

Using micromagnetic simulations, the behavior of magnetotactic bacteria in uniform magnetic fields can be successfully understood and deterministically controlled. Unlike magnetic field gradients, which attract all magnetosomes, the response of magnetotactic bacteria to uniform magnetic fields is determined by the arrangement of magnetosomes in the bacteria and how this arrangement is aligned relative to the forward direction of the bacteria. Most bacteria have long chains of magnetosomes which collectively behave like a uniaxial ferromagnet in strong uniform magnetic fields, and hence these bacteria either move parallel to the applied field or antiparallel to the applied field, with equal likelihood. This behavior is particularly useful when compared to other magnetic swimmers [36], as other magnetic swimmers require magnetic field gradients since they are not self-propelled.

Using external magnetic fields, the velocity vector of the bacteria can be changed from polar to nonpolar, individual bacteria and large groups of in-phase bacteria can be controlled with high precision, and nontrivial topological structures can be generated in both the polar and nonpolar velocity fields of the bacteria. This would also allow the manipulation and development of controlled active fluids dependent on these bacteria with viscosity and/or diffusivity regulated by the magnetic field [37].

We demonstrate two methods of controlling magnetotactic bacteria: external uniform fields to direct the bacteria as they self-propel and magnetic field gradients which pull the bacteria using attractive magnetic force. Previous work that deterministically controls magnetotactic bacteria relies on strong magnetic field gradients which vary over time. Having a large field gradient that penetrates several centimeters into biological material, such as those relied on for magnetic particle imaging [38] or magnetic resonance imaging, requires large electromagnets, extensive power electronics, and cooling systems. Electromagnets that generate uniform fields over similar spatial dimensions [39] do not require any of the above and are conveniently "table-top" (such as the one used in

this experiment). Having direct control of the bacteria using uniform magnetic fields effectively turns the bacteria into self-propelled microrobots, which could be used for a wide variety of *in vivo* applications, e.g., targeted drug delivery [40] or targeted magnetohyperthermia [41].

Genetically modifying magnetotatic bacteria to produce select arrangements of magnetosomes or controlling magnetosome growth in external fields [20] should allow for modification of bacterial properties in external fields. There is still much work to be done on understanding bacterium-bacterium interactions via the magnetic fields they produce. We hope this work inspires further research using uniform magnetic fields combined with other means of controlling magnetotactic bacteria (i.e., chemotaxis, microfluidics [5,6,29,41,43], etc.) to allow for novel applications.

#### ACKNOWLEDGMENTS

We thank the Bioelectronics group at MIT for their feedback on figures and use of BioRender. I.I.S. acknowledges the hospitality of the International Institute for Sustainability with Knotted Chiral Meta Matter (SKCM2) at Hiroshima University, Kavli Institute for Theoretical Physics at University of California at Santa Barbara and the Biosoft Centre at Tel Aviv University during his sabbatical visits, where he was partly working on this article. We would like to thank Dr. Elizabeth M. Jefremovas for her comments on the manuscript and thoughtful discussion on magnetotactic bacteria. The authors acknowledge the support of the U.S. Department of Energy Grant No. DE-SC0019306 (J.C., C.G., N.K., I.I.S.). Work at the Molecular Foundry was supported by the Office of Science, Office of Basic Energy Sciences, of the U.S. Department of Energy under Contract No. DE-AC02-05CH11231 (N.K., I.I.S.).

I.I.S. and N.K. conceptualized the project. C.G. and J.C. were responsible for the growth of bacterial colonies, bacterial strain selection, and provided microbiology expertise in analyzing the research results. N.K., B.S., and J.B.H. performed the TEM measurements. N.K. and B.S. performed the optical microscopy. N.K. did the figure design, magnetic simulations, and data analysis. All authors significantly contributed to the writing of the manuscript.

All authors declare they have no competing interests.

### DATA AVAILABILITY

The data are not publicly available. The data presented in this study as well as the mumax3 code are available from the contact author upon reasonable request.

<sup>[1]</sup> D. Faivre and D. Schüler, Chem. Rev. 108, 4875 (2008).

<sup>[2]</sup> M. L. Fdez-Gubieda et al., J. Appl. Phys. 128, 070902 (2020).

<sup>[3]</sup> J. J. Jacob and K. Suthindhiran, Mater. Sci. Eng. C 68, 919 (2016).

<sup>[4]</sup> J. F. Rupprecht, N. Waisbord, C. Ybert, C. Cottin-Bizonne, and L. Bocquet, Phys. Rev. Lett. 116, 168101 (2016).

<sup>[5]</sup> M. Marmol, E. Gachon, and D. Faivre, Rev. Mod. Phys. 96, 021001 (2024).

<sup>[6]</sup> J. Loehr, D. Pfeiffer, D. Schüler, and Th. M. Fischer, Soft Matter 12, 3631 (2016).

<sup>[7]</sup> B. Steinberger, N. Petersen, H. Petermann, and D. G. Weiss, J. Fluid Mech. 273, 189 (1994).

- [8] K. Erglis et al., Biophys. J. 93, 1402 (2007).
- [9] B. Vincenti, C. Douarche, and E. Clement, Phys. Rev. Fluids 3, 033302 (2018).
- [10] L. Le Nagard et al., Phys. Biol. 16, 066008 (2019).
- [11] N. Kent et al., Appl. Phys. Lett. 115, 112404 (2019).
- [12] N. Kent et al., Nat. Commun. 12, 1562 (2021).
- [13] J.-S. B. Tai, J.-S. Wu, and I. I. Smalyukh, Nat. Commun. 13, 2986 (2022).
- [14] I. I. Smalyukh, Rep. Prog. Phys. 83, 106601 (2020).
- [15] R. Moreno et al., J. Phys.: Condens. Matter 33, 175802 (2021).
- [16] See Supplemental Material at http://link.aps.org/supplemental/ 10.1103/ggl8-44wg for supplemental videos and figures.
- [17] M. Chariaou et al., Biophys. J. 108, 1268 (2015).
- [18] D. Gandia et al., Nanoscale 12, 16081 (2020).
- [19] C. Zahn et al., Sci. Rep. 7, 3558 (2017).
- [20] M. Blondeau et al., Sci. Rep. 8, 7699 (2018).
- [21] D. Bazylinski and R. Frankel, Nat. Rev. Microbiol. 2, 217 (2004).
- [22] C. T. Lefèvre and D. A. Bazylinski, Microbiol. Mol. Biol. Rev. 77, 1 (2013).
- [23] A. Farhan et al., Nat. Phys. 7, 75 (2011).
- [24] S. Velten et al., Appl. Phys. Lett. 110, 262406 (2017).
- [25] R. Streubel et al., Nano Lett. 18, 7428 (2018).
- [26] A. Vansteenkiste et al., AIP Advances 4, 107133 (2014).
- [27] O. Karaagac and H. Kockar, J. Magn. Magn. Mater. 409, 116 (2016).

- [28] S. J. Kemp, R. M. Ferguson, A. P. Khandhar, and K. M. Krishnan, RSC Adv. 6, 77452 (2016).
- [29] G. Lin, D. Makarov, and O. Schmidt, Lab Chip **17**, 1884 (2017).
- [30] E. Callaghan and S. Maslen, NASA Technical Note D-465 (Lewis Research Center, Cleveland Ohio, 1960).
- [31] H.-B. Braun, Adv. Phys. **61**, 1 (2012).
- [32] L. Meng, H.-H. Kim, H. Kim, M. Muhammed, and D. K. Kim, Nano. Rev. 1 (2010).
- [33] H. Iida, K. Takayanagi, T. Nakanishi, and T. Osaka, J. Colloid Interface Sci. 314, 274 (2007).
- [34] G. F. Goya, T. S. Berquó, F. C. Fonseca, and M. P. Morales, J. Appl. Phys. 94, 3520 (2003).
- [35] A. Akbarzadeh, M. Samiei, and S. Davaran, Nanoscale Res. Lett. 7, 3520 (2012).
- [36] A. Snezhko, M. Belkin, I. S. Aranson, and W.-K. Kwok, Phys. Rev. Lett. 102, 118103 (2009).
- [37] I. S. Aranson, Rep. Prog. Phys. 85, 076601 (2022).
- [38] Eli Mattingly et al., Phys. Med. Biol. 70, 015019 (2025).
- [39] J. L. Beckham et al., J. Am. Chem. Soc. 147, 13303 (2025).
- [40] D. Kuzajewska et al., Biology (Basel) 9, 102 (2020).
- [41] N. A. Usov, Nanomaterials (Basel) 10, 1320 (2020).
- [42] I. F. Sbalzarini and P. Koumoutsakos, J. Struct. Biol. 151, 182 (2005).
- [43] J. Noh, O. I. Osman, S. G. Aziz, P. Winget, and J. L. Brédas, Sci. Technol. Adv. Mater. 15, 044202 (2014).